coatings

MDPI

Article

Effects of Cr and Nb Additions on Sliding Wear Behaviors of the FePSiB Coatings

Yuan Feng [1], Jiangbo Cheng [1,2,*], Dan Liu [1] and Xiubing Liang [3,*]

[1] College of Mechanics and Materials, Hohai University, Nanjing 211100, China; fengyuan1995oppo@outlook.com (Y.F.); hhucjb199@hotmail.com (D.L.)
[2] Jiangsu Key Laboratory of Advanced Structural Materials and Application Technology, Nanjing 211167, China
[3] National Institute of Defense Technology Innovation, Academy of Military Sciences PLA China, Beijing 100010, China
* Correspondence: jiangbochenghhu@hotmail.com or chengjiangbo@hhu.edu.cn (J.C.); Liangxb_d@163.com (X.L.); Tel.: +86-25-8378-6046 (J.C.)

Received: 14 November 2018; Accepted: 13 December 2018; Published: 14 December 2018

Abstract: The tribological properties of the FePSiB amorphous/nanocrystalline coatings with Cr and Nb additions were investigated in reciprocating mode against tungsten carbide friction coupling with different dry sliding conditions. The wear rates of the FePSiB-based coatings increase linearly with the normal load and sliding speed. The coatings with Cr and Nb promote the formation of successive and compact oxide film on friction surface, which decreases significantly wear rate of the coating. Nano-mechanical characterization done to map the correlation between the elastic properties and wear resistance. The main damage mechanisms of the FePSiB-based coatings under dry friction conditions are abrasion wear, delamination failure and oxidation wear.

Keywords: coatings; dry friction; wear

1. Introduction

The discovery of metallic glass coating (MGCs) technology is a remarkable way of making use of the superior properties of amorphous alloys for structural applications [1–4]. MGCs have been proved an effective way to improve surface properties such as anti-corrosion and wear resistance [2–8]. These days, MGCs are used in the nuclear industry, power plants, marine engineering equipment, etc. [7–10].

In recent years, there has been sustainably rising demand for the development of high-performance coatings to resist various wear usefully. Owing to high strength, hardness and low cost, Fe-based MGCs have proposed a desirable wear resistant material [11]. The wear resistance of Fe-based MGCs acts as an important role for key equipment components applications with relative motions in service. Yugeswaran et al. [12] studied friction and wear performances of Fe-based MGCs containing TiN phase. The wear-resisting property of Fe-based MGCs increased by 2–3 times by the addition of Al_2O_3 particles in air and the NaCl solution [13]. Experiments by Zheng et al. [14] indicated that erosion–corrosion resistance of heat treated $Fe_{54.2}Cr_{18.3}Mo_{13.7}Mn_{2.0}W_{6.0}B_{3.3}C_{1.1}Si_{1.4}$ (wt.%) MGCs were better than the untreated one because of enhancement of hardness. Koga et al. [15] found that the wear resistant highly $Fe_{60}Cr_8Nb_8B_{24}$ amorphous coating was related to its high amorphous content, hardness and density. In our previous study, the dry sliding wear behaviors of the as-sprayed and devitrified FeBSiNb amorphous coatings were investigated [16,17]. In order to make the amorphous coating promise for practical applications, it is critical to develop new type high-performance coating material. Very recently, we have noticed that the amorphous alloys coatings in $Fe_{76}P_5Si_9B_{10}$ system present not only very low cost but also a critical solidification rate [18]. Although there have

been contrasting characterization results reported previously with different elements' additions, research on tribological behaviors and mechanisms of FePSiB-based amorphous and nanocrystalline coatings remains inadequate. Therefore, it is indispensable to investigate tribological properties of FePSiB-based amorphous and nanocrystalline coatings to further thoroughly comprehend their mechanical properties.

In the present paper, the effects of normal loads and sliding speeds on tribological performance of the FePSiB-based amorphous/nanocrystalline coatings were explored in detail. The worn morphologies of the coatings were characterized. The relationships between tribological behaviors and mechanical properties of the FePSiB-based amorphous/nanocrystalline coatings have been emphatically discussed.

2. Materials and Experimental Procedures

The $Fe_{76}P_5Si_9B_{10}$, $Fe_{66}P_5Si_9B_{10}Cr_{10}$ and $Fe_{65}P_5Si_9B_{10}Cr_{10}Nb_1$ cored wires were sprayed on Q235 steel substrate, respectively. The preparation process of the FePSiB-based core wires is as follows. At first, ball milling was employed to mix the alloy powders. After that, the steel strip was used to wrap the mixture alloys. Finally, the cored wires were drawn to the diameter of 2 mm. The details of the fabrication and characterizations of the FePSiB-based coatings are depicted in reference [18].

The nano-mechanical properties of the FePSiB-based coatings were measured on the cross section by Hysitron TriboIndenter (TI-750L, Hysitron, Inc., Minneapolis, MN, USA). The load of nanoindentation was 20 mN. The loading and unloading rate was 0.5 mN/s. To obtain the accuracy of the data, at least 15 indentations were performed for each loading. Simultaneously, Q235 steel was used as a comparison material.

Sliding reciprocating friction tests were executed by ball-on-block CETR Universal Tribometer (Bruker Nano Inc., Billerica, MA, USA). The friction coupling was tungsten carbide (WC) balls with a diameter of 12.7 mm. Before sliding test, WC balls and samples were ultra-sonicated in acetone solution for 10 min, and then dried. The sliding normal load was set to 20, 60 and 100 N. The reciprocating frequency was 6.25 Hz. The sliding speed was 25 mm/s. When different sliding speeds were being tested, the normal load was 60 N. The wear speed was 5, 25 and 45 mm/s with contrasting frequency of 1.25, 6.25 and 11.25 Hz, respectively. Experiments were operated in lab air. The stroke distance was 2 mm. The sliding wear time was 20 min and three times tests were carried out to get representative values for each testing conditions. After tests, volume loss was measured by an Olympus LEXT OL 3000-IR Infrared Confocal Microscope (Olympus America Inc., Center Valley, PA, USA). Wear rate was used to evaluate the wear resistance of the tested samples and it was calculated by the following equation:

$$\text{wear rate} = \frac{\text{Wear volume}}{\text{Sliding distance} \times \text{Normal load}} \quad (1)$$

The worn morphologies and chemical compositions were characterized by S3400 scanning electron microscopy (SEM, Hitachi, Ltd., Tokyo, Japan) and energy dispersive X-ray spectrometer (EDS, Hitachi, Ltd.).

3. Results and Discussion

3.1. Nano-Mechanical Properties

Figure 1 plots the loop curves of nanoindentation tests for the FePSiB-based coatings and Q235 steel substrate. Load-displacement curves show that the indentation of hard amorphous phase is shallower, while that of soft crystalline phase is deeper. These results are consistent with the microstructural reports in reference [18]. The maximum indentation displacement (h_{max}) of the $Fe_{76}P_5Si_9B_{10}$, $Fe_{66}P_5Si_9B_{10}Cr_{10}$ and $Fe_{65}P_5Si_9B_{10}Cr_{10}Nb_1$ coating are 311, 217 and 191 nm, respectively. With the addition of Cr and Nb, the maximum displacement of the FePSiB-based coating decreases gradually. The nano-hardness (H) and reduced Elastic Modulus (E_r) of the tested samples are listed in

Table 1. The additions of Cr and Nb excursions promote an increase in the *H*. The $Fe_{65}P_5Si_9B_{10}Cr_{10}Nb_1$ coating has a hardening response value of 7.7 GPa. This is ascribed to the higher amorphous content and the greater negative mixing enthalpy between Nb and P (Si, B) elements. It promotes the fracture strength of the FePSiB-based coatings, as supported by the investigations in reference [18,19]. Furthermore, with the addition of Cr and Nb elements, the E_r value of the FePSiB-based coatings is around 110 GPa, which is lower than that of the $Fe_{66}P_5Si_9B_{10}$ coating of 139 GPa. It is noted that the developed $Fe_{65}P_5Si_9B_{10}Cr_{10}Nb_1$ amorphous and nanocrystalline coating presents a higher hardness with a lower reduced Elastic Modulus. These data indicate that the coating has high wear and plastic deformation resistance [20].

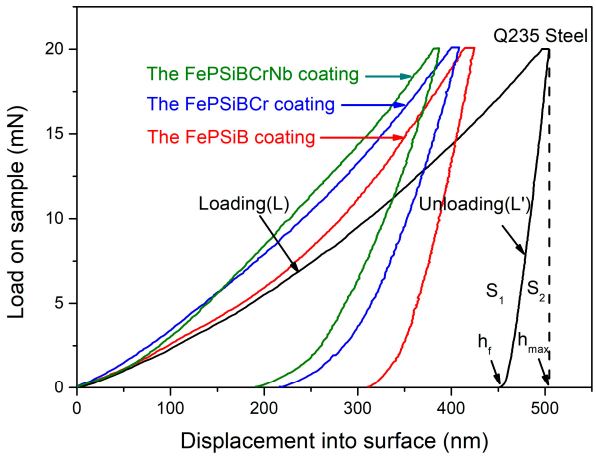

Figure 1. Load-unloading curves of the tested specimens.

Table 1. Nano-mechanical properties of the samples.

Samples	*H* (GPa)	E_r (GPa)	H/E_r	H^3/E_r^2	η (%)
Q235 steel substrate	3.0	210	0.014	0.0006	9.95
The FePBSi coating	5.5	139	0.040	0.009	24.4
The FePBSiCr coating	6.7	107	0.063	0.026	35.0
The FePBSiCrNb coating	7.7	108	0.071	0.039	39.4

Besides *H* and E_r, the H/E_r ratio and H^3/E_r^2 ratio values of the FePSiB-based coatings increase with the addition of Cr and Nb. Moreover, E_r values of the $Fe_{66}P_5Si_9B_{10}Cr_{10}$ and $Fe_{65}P_5Si_9B_{10}Cr_{10}Nb_1$ coating are 107 GPa and 108 GPa, respectively. There is no significant variation in E_r of both coatings. Therefore, η value can be employed to indicate how much elastic energy of the coatings can release after loading [21–23]. The η value confirms that the $Fe_{65}P_5Si_9B_{10}Cr_{10}Nb_1$ coating, where the amorphous and nanocrystalline structures coexist in the coating, appears optimum wear performance once more.

3.2. Friction and Wear Behaviors

The wear rates (W_R) and the coefficients of friction (*COF*) of the FePSiB-based coatings and Q235 steel substrate are illustrated in Figure 2. According to Figure 2a, it is evident that the W_R of the coatings depends on the normal loads and it increases with the increase of normal loads. The W_R of Q235 steel substrate is higher than the FePSiB-based coatings for all test conditions. The W_R of the FePSiB-based coatings decreases by the additions of Cr and Nb, When the load reaches 100 N, the wear resistance of the $Fe_{65}P_5Si_9B_{10}Cr_{10}Nb_1$ coating is about 1.7, 2.3 and 2.6 times that of the $Fe_{65}P_5Si_9B_{10}Cr_{10}$, $Fe_{65}P_5Si_9B_{10}$ coatings and Q235 steel substrate, respectively. The wear behaviors obey the traditional wear law governed by Archard's equation [24]:

$$dV = \frac{kP}{H}dx \quad (2)$$

where k is the wear resistance factor, P is the normal load, H is the hardness, dx is the differentiation of sliding wear distance, and dV is the differentiation of wear volume loss [24]. The Archard's equation illuminates the fact that the harder the material, the lower the wear mass loss. The wear rate of the FePSiB-based coatings is inversely proportional to the hardness under the same wear conditions. From Table 1, the $Fe_{65}P_5Si_9B_{10}Cr_{10}Nb_1$ coating has the highest hardness, so it presents the lowest W_R among the tested specimens.

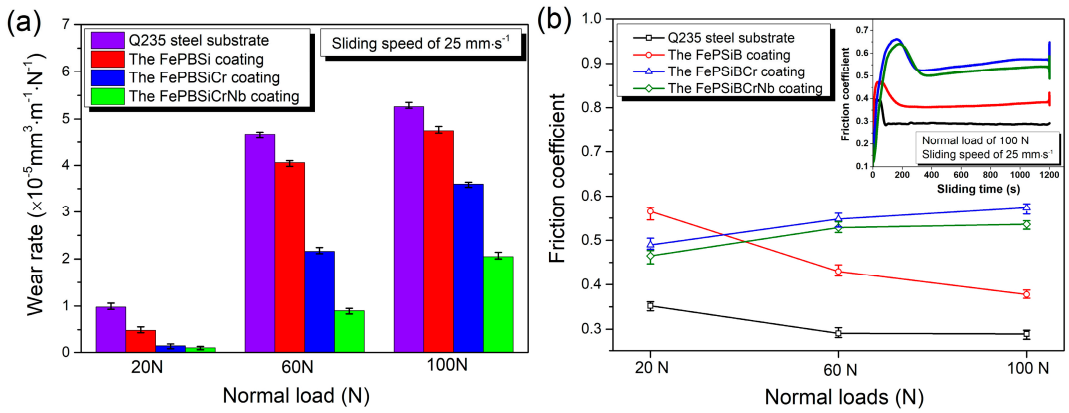

Figure 2. (**a**) Wear rates and (**b**) friction coefficients of the tested samples with different loads (v = 25 mm·s^{-1}).

Figure 2b plots the *COF* of all test samples. The *COF* of Q235 steel substrate is around 0.3–0.4, while that of the FePSiB-based coatings is about 0.4–0.6. The insert figure in Figure 2b depicts the *COF* curves of the tested samples at a sliding load of 100 N. The *COF* of the $Fe_{65}P_5Si_9B_{10}$ coating is decreasing with the increase of the normal loads. However, slight increments in the *COF* for the coatings with Cr and Nb additions are perceived. The *COF* of the $Fe_{65}P_5Si_9B_{10}$ coating is higher that of the coatings by the addition of Cr and Nb elements under a lower sliding load of 20 N. On the contrary, the $Fe_{65}P_5Si_9B_{10}$ coating presents the relatively lowest *COF* among the coatings as the normal load increases. This may be attributed to the nature of the soft and pliable debris. As discussed previously, the $Fe_{65}P_5Si_9B_{10}$ coating has a crystalline structure and a relatively low hardness [18]. At a lower load (20 N), the wear debris produced by the coating is relatively small, and little debris will be entrapped on the wear surface. Therefore, the wear surface of the coating with a lower hardness is prone to have greater roughness, so the *COF* is relatively high. As the load increases from 60 to 100 N, the FePSiB coatings are easy to form soft and ductile wear debris during sliding testing, which is easily involved on the worn surface to form tribo-film. These ductile tribo-films have a low shear stress, which leads to a lower *COF* at a higher normal load. Similar finding has reported recently by Ayyagari [25]. Therefore, the *COF* of the $Fe_{65}P_5Si_9B_{10}$ coating is lower at the higher applied load.

The W_R and *COF* of the coatings and the substrate with the variation of sliding speeds are shown in Figure 3. Similarly, as the sliding speed increases, the W_R of the tested samples increases. The Q235 steel substrate displays the highest W_R among all samples. With the addition of Cr and Nb, the W_R of the FePSiB-based coatings decreases, as depicted in Figure 3a. The main reason is that the temperature of the worn surface of the FePSiB-based coating will increase continuously with the increase of the sliding speed, resulting in a decrease in the hardness of the coating. Merchant et al. [26] investigated the fluctuation of hardness with the temperature originated from friction heat, and the relationship equation is listed as follows:

$$H = A\exp(-BT) \tag{3}$$

where T is the temperature, H is the hardness, and A is the intrinsic hardness when T equals zero and B is the softening coefficient. Equation (3) shows that the hardness of the FePSiB-based coatings decreases exponentially with the increase of worn surface temperature. Therefore, according to Archard's Equation (2), the W_R increases with the decrease of H. Moreover, as the Cr and Nb add to the

coating, the W_R of the coatings decreases under the same wear conditions. The $Fe_{65}P_5Si_9B_{10}Cr_{10}Nb_1$ coating exhibits the superior wear resistance. When sliding speed reaches 45 mm·s^{-1}, the W_R of the $Fe_{65}P_5Si_9B_{10}Cr_{10}Nb_1$ coating is about 1.7, 2.8 and 3.1 times that of the $Fe_{65}P_5Si_9B_{10}Cr_{10}$, $Fe_{65}P_5Si_9B_{10}$ coating and the Q235 steel substrate, respectively. Figure 3b and the insert figure shows the *COF* of the tested samples. The *COF* values for all samples reveal slight fluctuations with different sliding speeds. Similarly, the $Fe_{65}P_5Si_9B_{10}$ coating presents the lowest value among the FePSiB-based coatings.

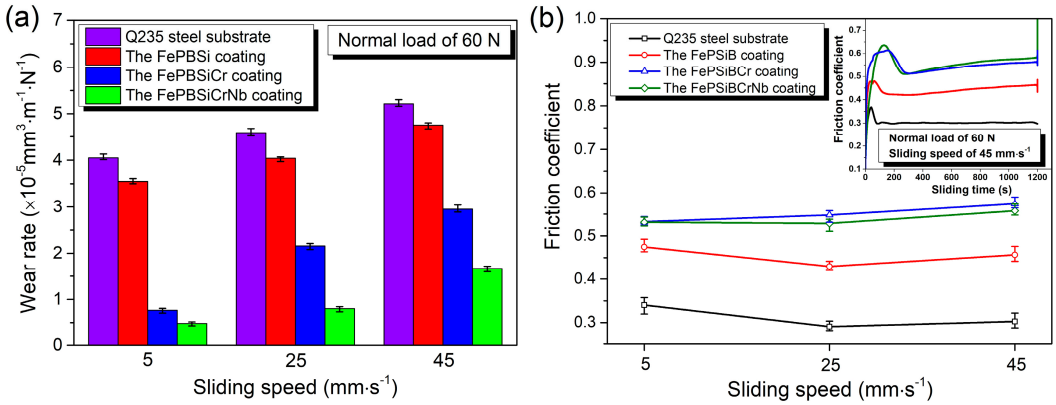

Figure 3. (**a**) Wear rates and (**b**) friction coefficients of the samples with various sliding speeds (P = 60 N).

3.3. Worn Morphology and Wear Mechanisms Analysis

Figure 4 shows the SEM image of worn morphologies of the FePSiB-based coatings and Q235 steel substrate with various sliding loads. For a Q235 steel substrate, the worn surface is rough and numerous wide and deep furrows appear on the worn surface at a load of 20 N, as seen with the arrow in Figure 4a. These grooves are likely formed when wear debris originated from the broken materials by continuous reciprocating sliding traps between the worn surface, counterface, and acts as fixed indenters. This is a three-body abrasive wear mechanism. For the $Fe_{65}P_5Si_9B_{10}$ coating in Figure 4b, besides several parallel furrows, there are some micro-cracks and big craters on the worn scar. This is also termed brittle fracture and delamination mechanism. Similar worn morphologies are observed for the $Fe_{65}P_5Si_9B_{10}Cr_{10}$ coating and the $Fe_{65}P_5Si_9B_{10}Cr_{10}Nb_1$ coating, but the plough groove morphologies are becoming narrow and shallow and the peeling-off appearance is not severe, as depicted in Figure 4c,d, respectively. With the addition of Cr and Nb, the worn surface of the coating is increasingly smooth, indicating less wear volume loss.

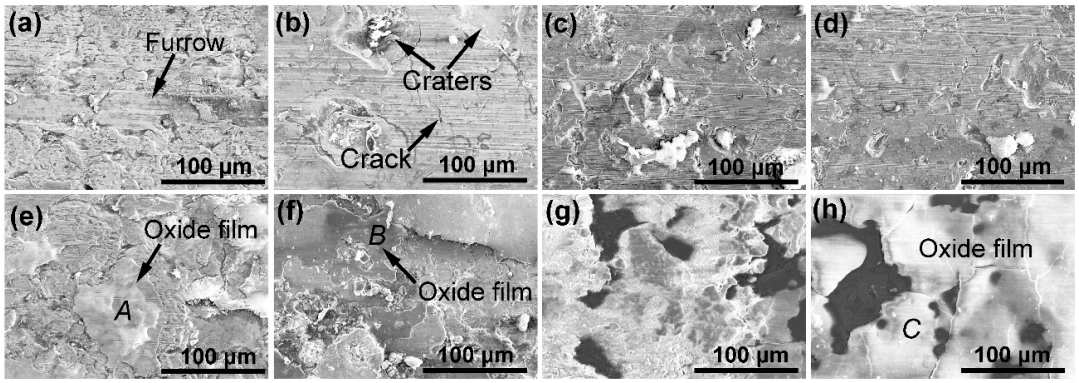

Figure 4. Worn surface of the coatings with different normal loads: (**a**) the substrate at 20 N; (**b**) the $Fe_{65}P_5Si_9B_{10}$ coating at 20 N; (**c**) the $Fe_{65}P_5Si_9B_{10}Cr_{10}$ coating at 20 N; (**d**) the $Fe_{65}P_5Si_9B_{10}Cr_{10}Nb_1$ coating at 20 N; (**e**) the substrate at 100 N; (**f**) the $Fe_{65}P_5Si_9B_{10}$ coating at 100 N; (**g**) the $Fe_{65}P_5Si_9B_{10}Cr_{10}$ coating at 100 N; and (**h**) the $Fe_{65}P_5Si_9B_{10}Cr_{10}Nb_1$ coating at 100 N.

When the sliding load is 100 N, the worn surface of the substrate is quite rough. Some discontinuous large islands of material are found on worn surfaces, seen in the "*A*" region in Figure 4e. The chemical compositions of the "*A*" region are $O_{66.56}$-$C_{5.55}$-$W_{3.53}$-$Fe_{24.37}$ (at.%). It means that the Q235 steel debris is entangled in the worn surface follow oxidation, which forms frictional oxide film. In addition, numerous furrows and craters are also observed on the worn surface of the substrate. For the $Fe_{65}P_5Si_9B_{10}$ coating, as shown in Figure 4f, many server splats fracture and big continuous craters display on the worn scars, confirming severe wear behavior of the coating. This is because the force per unit area of the surface of the coating increases sharply under a higher sliding load. After a long period of reciprocating sliding wear, the bonding strength between the inter-splats decreases and some splats are crushed out of the coating, resulting in the wear rate of the $Fe_{65}P_5Si_9B_{10}$ coating increasing. In addition, small-scale tearing tribological films (tribo-film) are found, seen in the "*B*" region in Figure 4f. The chemical composition of the "*B*" zone is $O_{62.61}$-$Si_{1.88}$-$C_{7.25}$-$W_{0.68}$-$Fe_{27.63}$ (at.%). It is also a frictional oxide layer.

For the $Fe_{65}P_5Si_9B_{10}Cr_{10}$ coating, some scuffing and locally loose tribo-film are found on the worn surface, as shown in Figure 4g. However, the worn scar of the $Fe_{65}P_5Si_9B_{10}Cr_{10}Nb_1$ coating is well distributed by the smooth bright tribo-film and no scoring marks could be observed, as shown in Figure 4h. In this situation, compared with the Figure 4f–g, the compact and continuous tribo-film covers a larger area in sliding track and no big spalling craters are detected, indicating more stability of the tribo-films. The chemical compositions of the mark "*C*" region are $O_{71.62}$-$Si_{1.64}$-$C_{4.42}$-$W_{2.11}$-$Fe_{16.66}$-$Cr_{3.03}$-$Nb_{0.52}$ (at.%). The oxidative tribo-film is produced by the following process. At first, when the elastic properties of the coating cannot tolerate its plastic deformation during sliding wear, debris will be formed. Some of this debris will be discharged from the worn surface, while others will remain by rolling with a WC ball. The retained wear debris undergoes repeated deformation and comminution. Simultaneously, the tribochemical reactions will rise during the formation of wear debris owing to friction heat. The higher the load, the bigger the flash temperature of the frictional surface, and the greater the tendency of oxidation debris. With the repeatedly smash and fragment of oxide debris, some fine debris will agglomerate adherent to the worn surface in some zone, especially in furrows or craters. Ultimately, the agglomerated fine oxide debris is compacted during reciprocating wear, thus forming a dense tribo-film. These oxidative tribo-films have two functions. Firstly, as abrasive particles between the sliding interface, it promotes three body wear, aggravates splats fracture and exacerbates volume loss (Figure 4e). Secondly, it plays a role of the protective tribo-film to prevent the wear of the coating. Therefore, few scuffing and scratching marks are visible on the worn scar of the $Fe_{65}P_5Si_9B_{10}Cr_{10}Nb_1$ coating (Figure 4h). However, shear stress and friction force cause mass loss of the coating [27]. Generally speaking, the higher the load, the greater the shear stress. The oxidative tribo-film easily delaminates under the action of greater external stress, which promotes the increase of wear rate. Therefore, the main wear mechanisms of the FePSiB-based coatings are delamination and oxidative wear.

Figure 5 is the cross-sectional worn morphologies of the FePSiB-based coatings with a load of 100 N. There is a big spalling carter in the $Fe_{65}P_5Si_9B_{10}$ coating (Figure 5a), suggesting the failure behavior of brittle spalling on this friction counterpart. In the early stage of sliding, the subsurface of the $Fe_{65}P_5Si_9B_{10}$ coating experiences elastoplastic deformation. Some microcracks will sprout at the edge of splats, oxides and unmelted particles. With the repeated squeezing of WC balls, the microcracks would propagate along the subsurface of the $Fe_{65}P_5Si_9B_{10}$ coating. The loose particles will peel off and crater forms. Moreover, there is a block-like, non-continuous substance existence in the crater, seen by "*A*" in Figure 5a. Table 2 lists its compositions. It is clear that the substance is oxidative tribo-film. For the $Fe_{65}P_5Si_9B_{10}Cr_{10}$ coating in Figure 5b, numerous transverse cracks and exfoliation appear in the worn track. This is mainly due to the shear stress produced in the sliding process. In addition, there is a thinner, continuous film in the "*B*" region in Figure 5b. The compositions in Table 2 confirm that it is an oxide film. However, with the addition of Nb element, the worn track is much smoother. Only some traversal micro-cracks and successive thick oxidative tribo-film marked "*C*" in Figure 5c

(the compositions are listed in Table 2) present in the subsurface. The composition marked "*C*" zone in Figure 5c is similar to that of the "*C*" region in Figure 4h, which further confirms the formation of friction oxide film. Moreover, with the additions of Cr and Nb, the cross-section analysis shows the oxide tribo-films on the worn surface tends to be thicker and denser, which results in a lower wear rate of the coatings under the same sliding testing conditions.

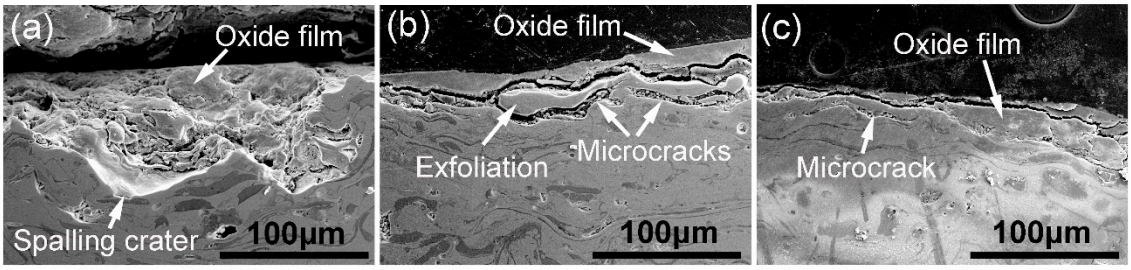

Figure 5. Cross-section worn morphologies of the coatings with load of 100 N. (**a**) $Fe_{65}P_5Si_9B_{10}$ coating; (**b**) $Fe_{65}P_5Si_9B_{10}Cr_{10}$ coating; and (**c**) $Fe_{65}P_5Si_9B_{10}Cr_{10}Nb_1$ coating.

Table 2. The compositions of worn surface.

Element (at.%)	O	C	Si	Cr	Nb	W	Fe
"*A*" region	62.61	7.25	1.88	–	–	0.63	Bal.
"*B*" region	72.48	3.37	2.14	2.84	–	2.1	Bal.
"*C*" region	72	4.51	1.71	3.04	0.4	2.29	Bal.

Figure 6 is the worn tracks of the FePSiB-based coatings and Q235 steel substrate with various sliding speeds at a load of 60 N. When the sliding speed is 5 mm·s^{-1}, some parallel furrows and severe scratches occur on the worn surface of the Q235 steel substrate, as shown in Figure 6a. As sliding speed reaches 45 mm·s^{-1}, the plough furrow appears on the worn surface along with the friction oxide film, as shown in Figure 6e.

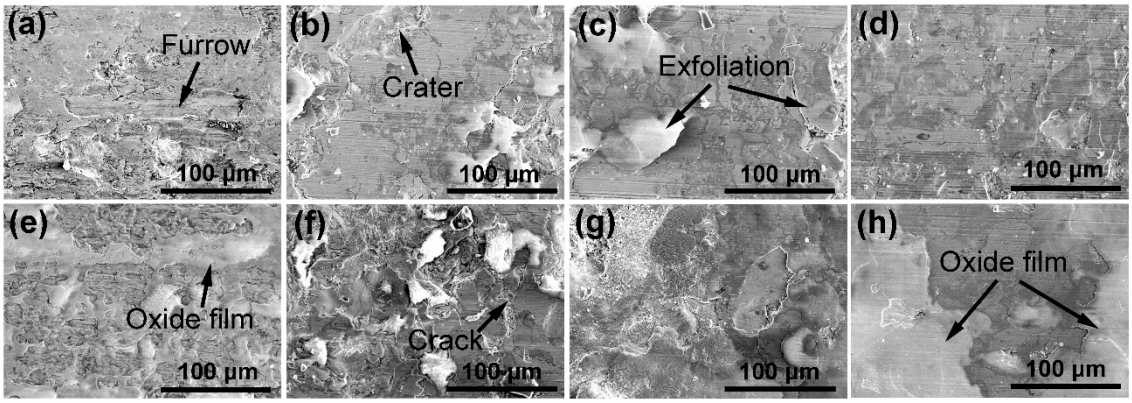

Figure 6. Worn surface of the coatings with various sliding speeds: (**a**) the substrate at 5 mm·s^{-1}; (**b**) the $Fe_{65}P_5Si_9B_{10}$ coating at 5 mm·s^{-1}; (**c**) the $Fe_{65}P_5Si_9B_{10}Cr_{10}$ coating at 5 mm·s^{-1}; (**d**) the $Fe_{65}P_5Si_9B_{10}Cr_{10}Nb_1$ coating at 5 mm·s^{-1}; (**e**) the substrate at 45 mm·s^{-1}; (**f**) the $Fe_{65}P_5Si_9B_{10}$ coating at 45 mm·s^{-1}; (**g**) the $Fe_{65}P_5Si_9B_{10}Cr_{10}$ coating at 45 mm·s^{-1}; and (**h**) the $Fe_{65}P_5Si_9B_{10}Cr_{10}Nb_1$ coating at 45 mm·s^{-1}.

Figure 6b,f are the worn scars of the $Fe_{65}P_5Si_9B_{10}$ coating. It can be seen that the parallel furrows present in the $Fe_{65}P_5Si_9B_{10}$ coating. In some places, the discontinuous white island-like tribo-films are found. Delamination appears on worn surfaces for all testing speed. With the increasing of sliding speed, the delamination becomes more severe. At a lower sliding speed, except slight furrow scratching, there is some exfoliation existence of the $Fe_{65}P_5Si_9B_{10}Cr_{10}$ coating, as can be seen from Figure 6c.

While some discontinuous black tribo-films with local spalling craters are observed at a higher sliding speed of 45 mm·s^{-1} (Figure 6g). For the $Fe_{65}P_5Si_9B_{10}Cr_{10}Nb_1$ coating in Figure 6d,h, the worn scar is smooth and no spalling craters appear. As sliding speed increases to 45 mm·s^{-1}, the oxide films become continuously and cover widely. The chemical compositions of the $Fe_{65}P_5Si_9B_{10}Cr_{10}Nb_1$ coating at speed of 5 and 45 m·s^{-1} are $O_{16.14}Si_{5.22}Cr_{10.12}Nb_{0.47}C_{9.79}Fe_{58.26}$ and $O_{45.27}Si_{3.08}Cr_{5.92}Nb_{0.4}C_{10.28}Fe_{35.05}$ (at.%), respectively. It can be seen that oxygen content is proportional to sliding speed. This is because the temperature at the interface depends on friction work, which is proportional to sliding speed and load. Therefore, the higher the sliding speed, the faster the formation of oxide film.

3D images of wear tracks developed after testing the coatings with various sliding speeds and normal loads are depicted in Figure 7. It is evident from the figure that the worn track of the $Fe_{65}P_5Si_9B_{10}$ coating is wide and deep. Compared Figure 7a with Figure 7d, wear marks of the coating with the addition of Cr and Nb is becoming much narrower and shallower than that of the $Fe_{65}P_5Si_9B_{10}$ coating. It further confirms that volume loss of the coatings containing Cr and Nb is less.

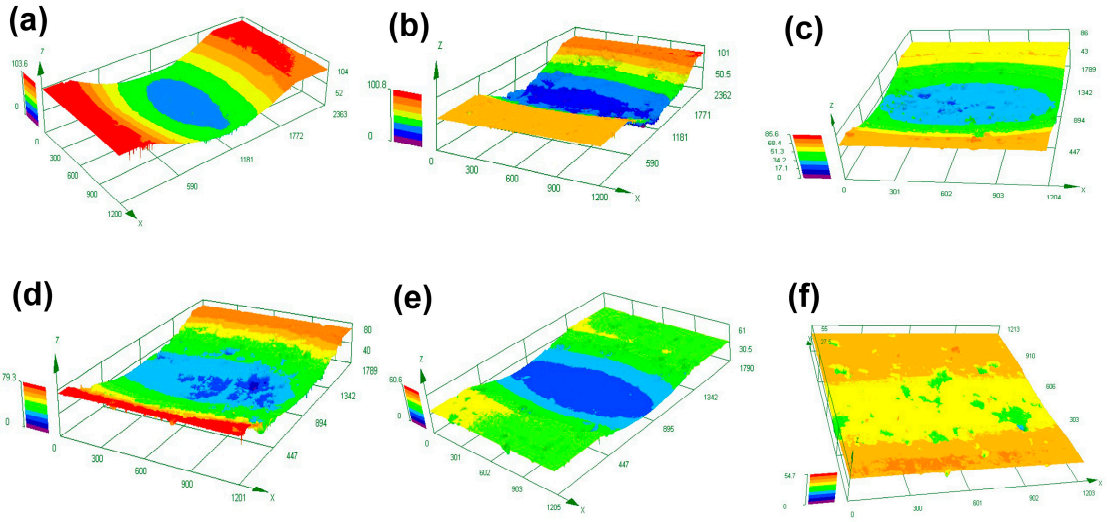

Figure 7. 3D morphologies of wear marks of (**a**) the $Fe_{65}P_5Si_9B_{10}$ coating at 100 N; (**b**) the $Fe_{65}P_5Si_9B_{10}Cr_{10}$ coating at 100 N; and (**c**) the $Fe_{65}P_5Si_9B_{10}Cr_{10}Nb_1$ coating at 100 N; (**d**) the $Fe_{65}P_5Si_9B_{10}$ coating at 45 mm·s^{-1}; (**e**) the $Fe_{65}P_5Si_9B_{10}Cr_{10}$ coating at 45 mm·s^{-1}; and (**f**) the $Fe_{65}P_5Si_9B_{10}Cr_{10}Nb_1$ coating at 45 mm·s^{-1}.

3.4. The Relationships between Microstructure, Mechanical Properties and Wear Resistance

From the above observation of wear experiment results, it can be deduced that the $Fe_{65}P_5Si_9B_{10}Cr_{10}Nb_1$ coating displays superior wear resistance compared with the $Fe_{65}P_5Si_9B_{10}$ coating and $Fe_{65}P_5Si_9B_{10}Cr_{10}$ coating. The microstructure and mechanical properties of the FePSiB-based coatings are responsible for their wear resistance. Firstly, through previous investigations [14], the $Fe_{65}P_5Si_9B_{10}$ coating has α-Fe phase nanoscale structure. The additions of Cr and Nb promote the decreasing size of crystalline and the formation of a full amorphous phase. It is beneficial to improving the wear resistance of the coating with nanoparticles distributing uniform in amorphous matrix [28]. According to the Hall–Petch formula, the smaller the grain size, the higher the hardness and strength of the coating. The high-density grain boundaries and phase interfaces between nanocrystalline have a positive impact on preventing the propagation of cracks and improving the fatigue life of coatings. Simultaneously, with the increasing of amorphous fraction in the $Fe_{65}P_5Si_9B_{10}Cr_{10}Nb_1$ coating, the residual compressive stress and local shear band actions of amorphous structure also contribute to the enhancement of wear resistance [29]. Secondly, compared with the $Fe_{65}P_5Si_9B_{10}$ and $Fe_{65}P_5Si_9B_{10}Cr_{10}$ coatings, the $Fe_{65}P_5Si_9B_{10}Cr_{10}Nb_1$ coating has better mechanical properties. Figure 8a,b depict the relationships between the H/E_r ratio, the H^3/E_r^2 ratio and wear rates for the coatings with a sliding load of 60 N and speed of 25 mm·s^{-1}. It is clear that the wear rate is decreasing

as a function of the H/E_r and H^3/E_r^2 ratio. The reason is due to the higher H/E_r ratio and the H^3/E_r^2 ratio providing the greater load-bearing capacity of the coating. Thus, when the WC ball slides on the FePSiB-based coatings, the load-bearing capacity of the coating is large enough to tolerate external loading without exceeding its elastic limit, which increases wear resistance. The relationship between H/E_r and elastic recovery η value is shown in Figure 8c. The H/E_r ratio is proportional to η value because they are the elastic property index of materials. The high η value and the H/E_r ratio endue the $Fe_{65}P_5Si_9B_{10}Cr_{10}Nb_1$ coating with greater deformation resistance, higher strain tolerance and less damage.

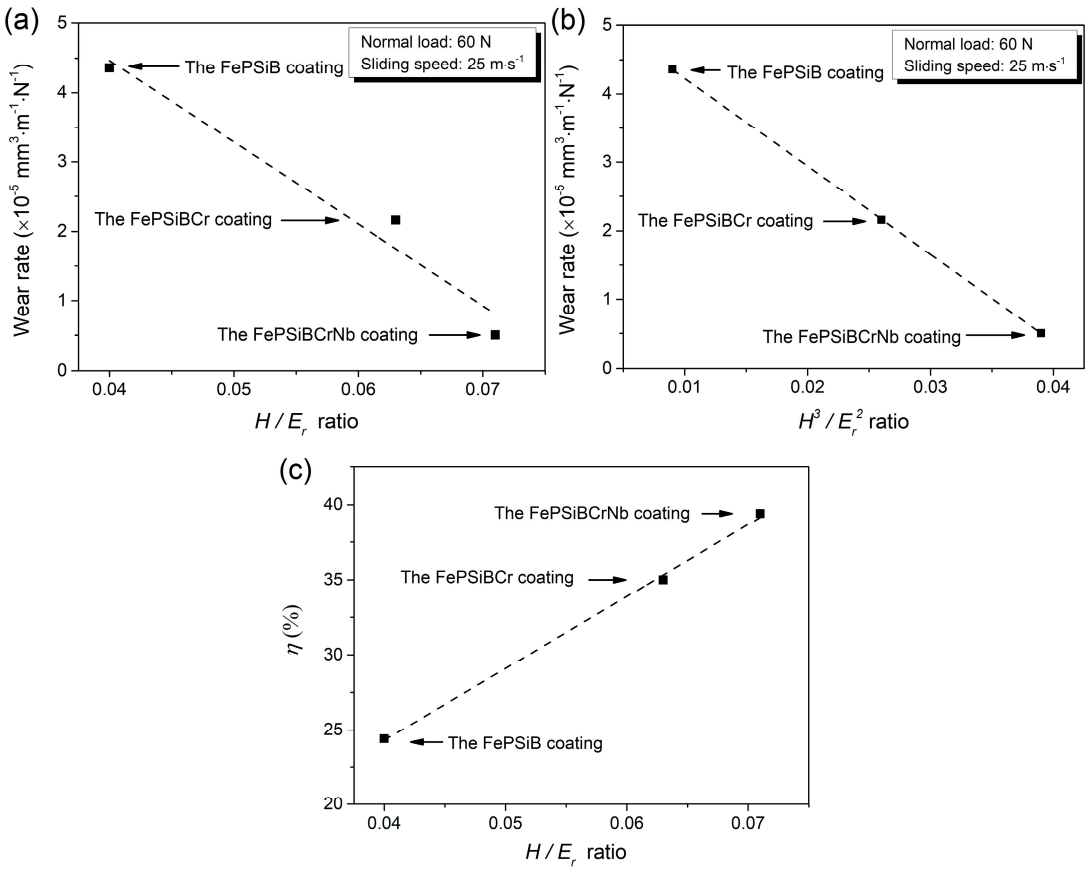

Figure 8. (**a**) the relationships between the H/E_r ratio and wear rate; (**b**) the relationships between the H^3/E_r^2 ratio and wear rate; and (**c**) the relationships between the H/E_r ratio and η value.

Thirdly, the larger area and compact oxide tribo-films are formed on the $Fe_{65}P_5Si_9B_{10}Cr_{10}Nb_1$ coating through the subsequently sliding wear process to protect the underlying coating from further wear. Consequently, it avoids the direct WC ball-to-coating contact and results in a relatively low wear rate. This result is consistent with the morphologies revealed in Figures 4–6. It is suggested that the formation of dense oxide films on the worn surface is propitious to reducing volume loss and protecting the sliding surface of components under dry friction conditions. Therefore, the wear resistance of the coating containing Cr and Nb increases gradually.

4. Conclusions

The wear behaviors of FePSiB-based coatings were investigated under dry sliding reciprocating conditions. The wear rates of the FePSiB-based coating increase linearly with the increasing of sliding loads and speeds. The additions of Cr and Nb improve significantly the frictional performance of the FePSiB coating. When the load reaches 100 N, the relative wear resistance of the $Fe_{65}P_5Si_9B_{10}Cr_{10}Nb_1$ coating is about 1.7, 2.3 and 2.6 times that of the $Fe_{65}P_5Si_9B_{10}Cr_{10}$, $Fe_{65}P_5Si_9B_{10}$ coatings and Q235

steel substrate with a sliding load of 100 N and speed of 25 mm·s^{-1}, respectively. The analysis of worn morphologies shows that the high sliding load and speed promote the formation of oxide films. The coverage region and stability of the oxide tribo-films in the coating containing Cr and Nb increase gradually under the same dry sliding conditions. The successive and compact oxide tribo-film is propitious to wear resistance. The main wear behaviors of the FePSiB-based coatings are abrasive wear, delamination and oxidation wear. The $Fe_{65}P_5Si_9B_{10}Cr_{10}Nb_1$ coating has superior wear resistance because of finer nanocrystalline, residual full amorphous matrix, excellent elastic recovery properties and dense oxide tribo-films.

Author Contributions: X.L. and J.C. conceived and designed the experiments; D.L. and Y.F. performed the experiments; D.L. analyzed the data; Y.F. and J.C. wrote and revised the paper.

Funding: This research was funded by the National Natural Science Foundation of China (No. 51575159), the Key Research and Development plan of Jiangsu Province, China (No. BE2017065), the Fundamental Research Funds for the Central Universities (No. 2018B16914), and the Opening Project of Jiangsu Key Laboratory of Advanced Structural Materials and Application Technology (No. ASMA201801).

Conflicts of Interest: The authors declare no conflict of interest.

References

1. Joshi, S.S.; Katakam, S.; Singh Arora, H.; Mukherjee, S.; Dahotre, N.B. Amorphous coatings and surfaces on structural materials. *Crit. Rev. Solid State Mater. Sci.* **2016**, *41*, 1–46. [CrossRef]
2. Balla, V.K.; Bandyopadhyay, A. Laser processing of Fe-based bulk amorphous alloy. *Surf. Coat. Technol.* **2010**, *205*, 2661–2667. [CrossRef]
3. Kobayashi, A.; Kuroda, T.; Kimura, H.; Inoue, A. Effect of Zr on microstructure of metallic glass coatings prepared by gas tunnel type plasma spraying. *J. Nanosci. Nanotechnol.* **2012**, *12*, 4883–4886. [CrossRef] [PubMed]
4. Zhou, Y.Y.; Ma, G.Z.; Wang, H.D.; Li, G.L.; Chen, S.Y.; Wang, H.J. Fabrication and characterization of supersonic plasma sprayed Fe-based amorphous metallic coatings. *Mater. Des.* **2016**, *110*, 332–339. [CrossRef]
5. Sahasrabudhe, H.; Bandyopadhyay, A. Laser processing of Fe based bulk amorphous alloy coating on zirconium. *Surf. Coat. Technol.* **2014**, *240*, 286–292. [CrossRef]
6. Sahasrabudhe, H.; Dittrick, S.A.; Bandyopadhyay, A. Laser processing of Fe-based bulk amorphous alloy coatings on titanium. *Metall. Mater. Trans. A* **2013**, *44*, 4914–4926. [CrossRef]
7. Guo, S.F.; Pan, F.S.; Zhang, H.J.; Zhang, D.F.; Wang, J.F.; Miao, J.; Su, C.; Zhang, C. Fe-based amorphous coating for corrosion protection of magnesium alloy. *Mater. Des.* **2016**, *108*, 624–631. [CrossRef]
8. Blink, J.; Farmer, J.; Choi, J.; Saw, C. Applications in the nuclear industry for thermal spray amorphous metal and ceramic coatings. *Metall. Mater. Trans. A* **2009**, *40*, 1344–1354. [CrossRef]
9. Luding, R.; Thorpe, R. Electric arc spray coatings increase cost and reliability of power generation systems. *Adv. Mater. Process.* **2013**, *171*, 46–48.
10. Cheng, J.B.; Liang, X.B.; Chen, Y.X.; Wang, Z.H.; Xu, B.S. High-temperature erosion resistance of FeBSiNb amorphous coatings deposited by arc spraying for boiler applications. *J. Therm. Spray Technol.* **2013**, *22*, 820–827. [CrossRef]
11. Suryanarayana, C.; Inoue, A. Iron-based bulk metallic glasses. *Int. Mater. Rev.* **2013**, *58*, 131–166. [CrossRef]
12. Yugeswaran, S.; Kobayashi, A.; Suresh, K.; Subramanian, B. Characterization of gas tunnel type plasma sprayed TiN reinforced Fe-based metallic glass coatings. *J. Alloy. Compd.* **2013**, *551*, 168–175. [CrossRef]
13. Yasir, M.; Zhang, C.; Wang, W.; Xu, P.; Liu, L. Wear behaviors of Fe-based amorphous composite coatings reinforced by Al_2O_3 particles in air and in NaCl solution. *Mater. Des.* **2015**, *88*, 207–213. [CrossRef]
14. Zheng, Z.B.; Zheng, Y.G.; Sun, W.H.; Wang, J.Q. Effect of heat treatment on the structure, cavitation erosion and erosion–corrosion behavior of Fe-based amorphous coatings. *Tribol. Int.* **2015**, *90*, 393–403. [CrossRef]
15. Koga, G.Y.; Schulz, R.; Savoie, S.; Nascimento, A.R.C.; Drolet, Y.; Bolfarini, C.; Kiminami, C.S.; Botta, W.J. Microstructure and wear behavior of Fe-based amorphous HVOF coatings produced from commercial precursors. *Surf. Coat. Technol.* **2017**, *309*, 938–944. [CrossRef]
16. Cheng, J.B.; Liang, X.B.; Xu, B.S. Devitrification of arc-sprayed FeBSiNb amorphous coatings: Effects on wear resistance and mechanical behavior. *Surf. Coat. Technol.* **2013**, *235*, 720–726. [CrossRef]

17. Cheng, J.; Liu, D.; Liang, X.; Chen, Y. Wear behaviors of arc-sprayed FeBSiNb amorphous coatings. *Tribol. Lett.* **2015**, *60*, 22. [CrossRef]
18. Cheng, J.; Zhao, S.; Liu, D.; Feng, Y.; Liang, X. Microstructure and fracture toughness of the FePSiB-based amorphous/nanocrystalline coatings. *Mate. Sci. Eng. A* **2017**, *696*, 341–347. [CrossRef]
19. Takeuchi, A.; Inoue, A. Classification of bulk metallic glasses by atomic size difference, heat of mixing and period of constituent elements and its application to characterization of the main alloying element. *Mater. Trans.* **2005**, *46*, 2817–2829. [CrossRef]
20. Nishikawa, M.; Soyama, H. Two-step method to evaluate equibiaxial residual stress of metal surface based on micro-indentation tests. *Mater. Des.* **2011**, *32*, 3240–3247. [CrossRef]
21. Leyland, A.; Matthews, A. On the significance of the H/E ratio in wear control: A nanocomposite coating approach to optimised tribological behaviour. *Wear* **2000**, *246*, 1–11. [CrossRef]
22. Jeong, D. Abrasive Wear Behaviour of Electrodeposited Nanocrystalline Materials. Ph.D.Thesis, University of Toronto, Toronto, ON, Canada, 2003.
23. Dao, M.; Lu, L.; Asaro, R.J.; De Hosson, J.T.M.; Ma, E. Toward a quantitative understanding of mechanical behavior of nanocrystalline metals. *Acta Mater.* **2007**, *55*, 4041–4065. [CrossRef]
24. Archard, J.F. Contact and rubbing of flat surface. *J. Appl. Phys.* **1953**, *24*, 981–988. [CrossRef]
25. Ayyagari, A.; Scharf, T.W.; Mukherjee, S. Dry reciprocating sliding wear behavior and mechanisms of bulk metallic glass composites. *Wear* **2016**, *350–351*, 56–62. [CrossRef]
26. Merchant, H.D.; Murty, G.S.; Bahadur, S.N.; Dwivedi, L.T.; Mehrotra, Y. Hardness-temperature relationships in metals. *J. Mater. Sci.* **1973**, *8*, 437–442. [CrossRef]
27. Suh, N.P. *Tribophysics*; Prentice-Hall: Englewood Cliffs, NJ, USA, 1986.
28. Cheng, J.; Liang, X.; Xu, B.; Wu, Y. Formation and properties Fe-based amorphous/nanocrystalline coating prepared by wire arc spraying process. *J. Non-Cryst. Solids* **2009**, *355*, 1673–1678. [CrossRef]
29. Kim, Y.H.; Higara, K.; Inoue, A.; Masumoto, T.; Jo, H.H. Crystallization and high mechanical strength of Al-based amorphous alloys. *Mater. Trans. JIM* **1994**, *35*, 293–302. [CrossRef]